Copper Nanowire–Graphene Core–Shell Nanostructure for Highly Stable Transparent Conducting Electrodes

Yumi Ahn,† Youngjun Jeong,† Donghwa Lee, and Youngu Lee*

Department of Energy Systems Engineering, Daegu Gyeongbuk Institute of Science and Technology (DGIST), 50-1 Sang-Ri, Hyeonpung-Myeon, Dalseong-Gun, Daegu 711-873, Korea. †These authors contributed equally.

ABSTRACT A copper nanowire–graphene (CuNW-G) core–shell nanostructure was successfully synthesized using a low-temperature plasma-enhanced chemical vapor deposition process at temperatures as low as 400 °C for the first time. The CuNW-G core–shell nanostructure was systematically characterized by scanning electron microscopy, transmission electron microscopy, X-ray diffraction, Raman, and X-ray photoelectron spectroscopy measurements. A transparent conducting electrode (TCE) based on the CuNW-G core–shell nanostructure exhibited excellent optical and electrical properties compared to a conventional indium tin oxide TCE. Moreover, it showed remarkable thermal oxidation and chemical stability because of the tight encapsulation of the CuNW with gas-impermeable graphene shells. The potential suitability of CuNW-G TCE was demonstrated by fabricating bulk heterojunction polymer solar cells. We anticipate that the CuNW-G core–shell nanostructure can be used as an alternative to conventional TCE materials for emerging optoelectronic devices such as flexible solar cells, displays, and touch panels.

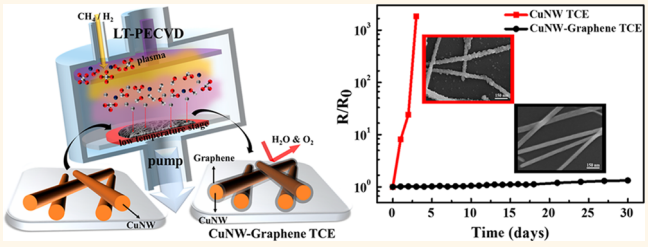

KEYWORDS: copper nanowire · graphene · core–shell · transparent conducting electrode · polymer solar cell

Transparent conducting electrodes (TCEs) based on indium tin oxide (ITO) have been widely used as an essential element of various optoelectronic devices, including liquid crystal displays (LCDs), organic light-emitting diodes (OLEDs), touch screen panels (TSPs), and solar cells.[1,2] Vacuum-deposited ITO possesses good physical properties such as high optical transmittance and low sheet resistance as a TCE for various optoelectronic devices. However, it has several drawbacks such as brittleness, low optical transmittance, high refractive index, and high processing temperature.[3,4] Furthermore, the price of ITO has been highly volatile recently, due to the scarcity of indium resources and the increased consumption of the material. Therefore, cheap, flexible, and solution-processed TCEs have been required for next generation optoelectronic devices such as flexible solar cells and displays.[5–7] Recently, silver nanowire (AgNW) TCEs showed optical and electrical performance superior to that of ITO.[8–12] However, the mass production of AgNWs is limited by its price ($505 USD/kg) and scarcity. Copper is 1000 times more abundant and 80 times less expensive ($6.36 USD/kg) than silver.[13] Moreover, the electrical resistivity of copper (16.8 nΩ·m) is as low as that of silver, which has the lowest electrical resistivity (15.9 nΩ·m). Therefore, a copper nanowire (CuNW) TCE has attracted considerable interest as a potential alternative to ITO and AgNW TCEs. More recently, researchers have shown that CuNW TCEs can possess remarkable physical properties such as excellent electrical conductivity, optical transparency, and mechanical flexibility.[14–16] However, there is still an issue regarding long-term stability, which makes it difficult for practical use. For instance, a CuNW is easily oxidized when exposed to air even at room temperature, leading to a sharp increase in sheet resistance and haziness of the CuNW TCE. Thus, it is necessary to suppress the oxidation of the CuNW in order to

* Address correspondence to youngulee@dgist.ac.kr.

Received for review January 5, 2015 and accepted February 20, 2015.

Published online February 24, 2015
10.1021/acsnano.5b00053

enhance the long-term stability of CuNW TCEs. Recently, many efforts have been made to develop novel protection layers for CuNW TCEs. Several approaches have been used to address this issue, including aluminum-doped zinc oxide/aluminum oxide coating, nickel electroless deposition, and polymer protection layers.[17−19] However, these protection layers tend to cause a rough surface morphology, inefficient electrical connection, and diminished optoelectronic properties of CuNW TCEs. The intrinsic drawback of CuNW TCEs has not been completely solved. Therefore, the challenge still remains to develop a new protection layer which is cheap, gas-impermeable, and electrically conductive while maintaining optoelectronic properties and low cost.

Recently, we successfully demonstrated a graphene protection layer for AgNW TCEs because the graphene has extraordinary gas-impermeability as well as electrical conductivity.[20] However, it is very difficult to employ the graphene as a protection layer for CuNW TCEs in ambient conditions due to the oxidation issue. An ideal approach to protect a CuNW from its oxidation is to synthesize a CuNW−graphene (CuNW-G) core−shell nanostructure in which the CuNW is tightly encapsulated with gas-impermeable graphene shells. This approach could guarantee not only optoelectronic properties of CuNW TCEs but also highly enhanced long-term stability. However, to the best of our knowledge, it is impossible to grow the graphene directly onto CuNW because a conventional thermal chemical vapor deposition (T-CVD) process is restricted to a high process temperature limit of around 1000 °C for graphene synthesis.[21]

A plasma-enhanced CVD (PECVD) process is of particular interest due to its wide applicability for various thin film deposition and synthesis of nanomaterials.[22] Compared to the conventional T-CVD process, it has several advantages such as low-temperature processing, fast deposition rate, composition controllability, and good uniformity because of the reactive gas species produced by high-density plasmas. Thus, it has been widely used as an industrial process for various electronic applications such as displays, semiconductors, and solar cells.[23] More recently, it is reported that monolayer graphene and few-layer graphene were synthesized onto a Cu film by the PECVD process at a relatively low temperature.[24,25]

Herein, we introduce a copper nanowire−graphene (CuNW-G) core−shell nanostructure by a low-temperature PECVD (LT-PECVD) process and its application for transparent conducting electrodes. The CuNW-G core−shell nanostructure was successfully prepared by a LT-PECVD process at temperatures as low as 400 °C for the first time. A TCE based on the CuNW-G core−shell nanostructure exhibited excellent optical and electrical properties comparable to those of conventional ITO. In addition, it showed remarkable thermal oxidation and chemical stability because of the tight encapsulation of the CuNW with gas-impermeable graphene shells. The potential suitability of the CuNW-G nanostructure-based TCE was demonstrated by fabricating bulk heterojunction polymer solar cells (PSCs). We anticipate that the CuNW-G core−shell nanostructure can be used as an alternative to conventional TCE materials for emerging optoelectronic devices such as flexible solar cells, displays, and touch panels.

RESULTS AND DISCUSSION

In order to fabricate a CuNW TCE with excellent optoelectronic properties such as high optical transmittance and low sheet resistance, it is crucial to decrease the number of junctions between CuNWs and increase open areas in the conductive CuNW network. Thus, longer and thinner CuNWs need to be synthesized for fewer junctions and lower percolation threshold. Therefore, we performed the synthesis of a longer and thinner CuNW using reduction of a Cu(II) ion from $CuCl_2 \cdot 2H_2O$ to Cu(0) in an aqueous solution with glucose and hexadecylamine (HDA) as reducing and capping reagents, respectively. The average length and diameter of synthesized CuNWs are 30 ± 13 μm and 36 ± 5 nm, respectively (Supporting Information Figure S1). It is also found that the concentration of HDA plays a crucial role in controlling the shape of copper nanostructures (Figure S2).

Figure 1a shows a photograph of the LT-PECVD system for the synthesis of the CuNW-G core−shell nanostructure. Figure 1b presents a schematic illustration for the synthesis of the CuNW-G core−shell nanostructure by the LT-PECVD process. To fabricate a CuNW-G core−shell nanostructure, a CuNW on a glass substrate was placed in a vacuum PECVD chamber (5.0×10^{-6} Torr) and heated to a process temperature ranging from 400 to 800 °C. We applied a hydrogen plasma with a radio frequency (RF) power of 50 W in order to remove an oxide layer and other contaminants on the surface of the CuNW. Then, we introduced a reaction gas mixture composed of methane and hydrogen (CH_4/H_2 = 40:1, 120 sccm) into the chamber. We then performed PECVD at 1.0×10^{-3} Torr with RF power of 50 W for various process time ranging from 3 to 9 min and cooled to room temperature.

To evaluate the morphology change of the CuNW after the LT-PECVD process, the surface of the CuNW was investigated using scanning electron microscopy (SEM). As shown in Figure S4, the CuNW treated with the LT-PECVD at process temperatures as high as 600 °C is partially melted and structurally damaged. It is well-known that the CuNW possesses a relatively lower melting point because of a size effect, even though the melting point of bulk copper is 1084 °C. As a result, the CuNW could be damaged by thermal stress at processing temperatures as high as 600 °C.

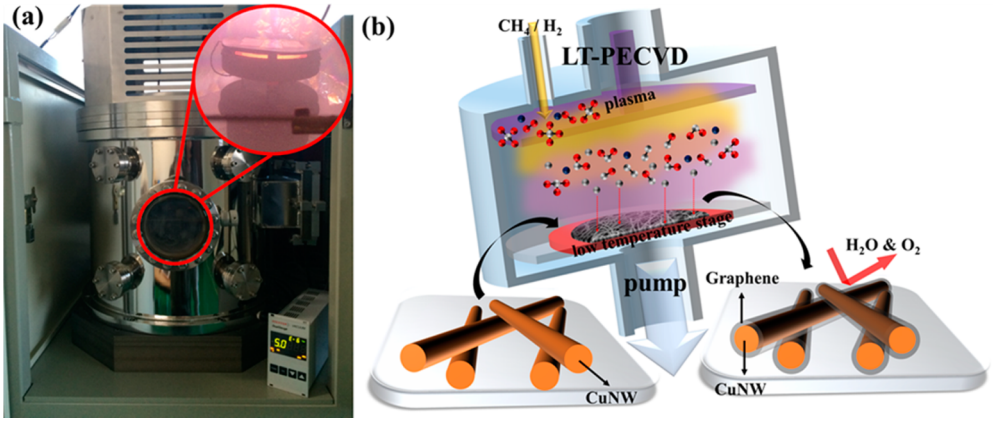

Figure 1. (a) Photograph of the LT-PECVD system for the synthesis of CuNW-G core−shell nanostructure. Inset: Generated radio frequency plasma. (b) Schematic illustration for the synthesis of the CuNW-G core−shell nanostructure by the LT-PECVD process.

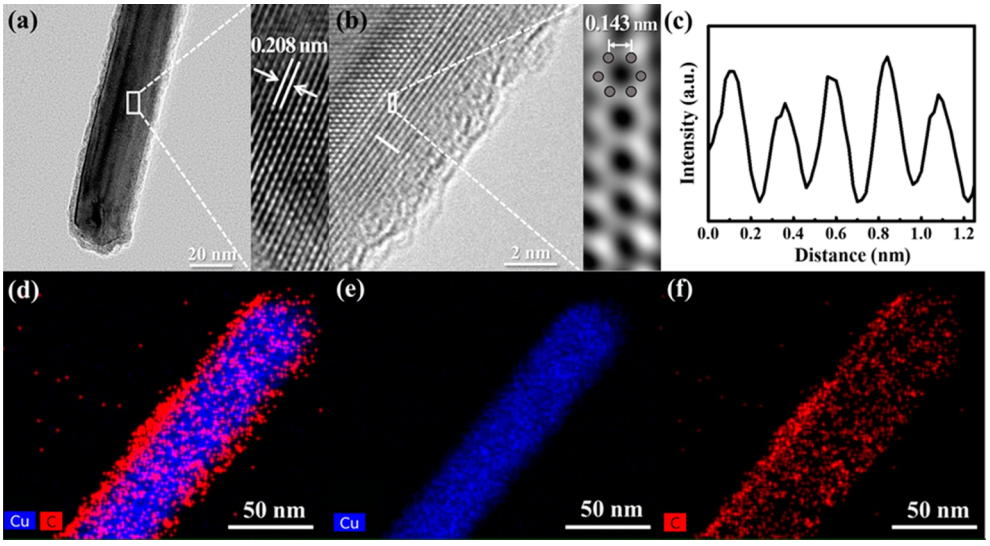

Figure 2. (a) TEM image of CuNW-G core−shell nanostructure. Inset: High-resolution TEM image of the middle of CuNW-G core−shell nanostructure. (b) High-resolution TEM image of the edge of CuNW-G core−shell nanostructure. Inset: Inverse FFT image. (c) Line intensity profile along the selected line of the CuNW-G core−shell nanostructure. (d) EDS mapping analysis of CuNW-G core−shell nanostructure. (e) Cu elemental mapping and (f) carbon elemental mapping over the CuNW-G core−shell nanostructure.

On the other hand, when the CuNW is treated with the LT-PECVD at process temperatures as low as 500 °C, the morphology of the CuNW is retained without any structural damage. Moreover, the SEM image clearly shows the fused junction at the CuNW intersection, which can reduce the typical high junction resistance between CuNWs (Figure S5). Thus, we performed the LT-PECVD process at process temperatures as low as 500 °C to grow a graphene layer directly onto the CuNW for the synthesis of a CuNW-G core−shell nanostructure.

Transmission electron microscopy (TEM) and energy-dispersive spectroscopy (EDS) mapping analysis were performed to characterize the phase identity and chemical composition of the CuNW treated with the LT-PECVD process, as shown in Figure 2. The TEM image clearly exhibits that the CuNW is fully covered with 10−15 layers of which the thickness is about 5 nm (Figure S6). Moreover, EDS mapping analysis indicates that a thin carbon nanostructure is coated along the surface of the CuNW, suggesting the successful formation of the CuNW-G core−shell nanostructure. In order to characterize the phase identity of the CuNW-G core−shell nanostructure, we measured TEM on the middle and edge of the CuNW-G core−shell nanostructure. Figure 2a shows a TEM image that was taken from the middle of the CuNW-G core−shell nanostructure. The CuNW lattice is strongly observed on the middle of the CuNW-G core−shell nanostructure. The lattice distance is 0.208 nm, corresponding to the lattice distance value of the (111) plane of the CuNW. On the other hand, at the edge of CuNW-G core−shell nanostructure, only graphene layers are observed (Figure 2b). Figure 2c shows the intensity profile from single pixel line. The lattice constant of the graphene shell is estimated to be 0.246 nm, which is almost similar to the theoretical value of the zigzag orientation

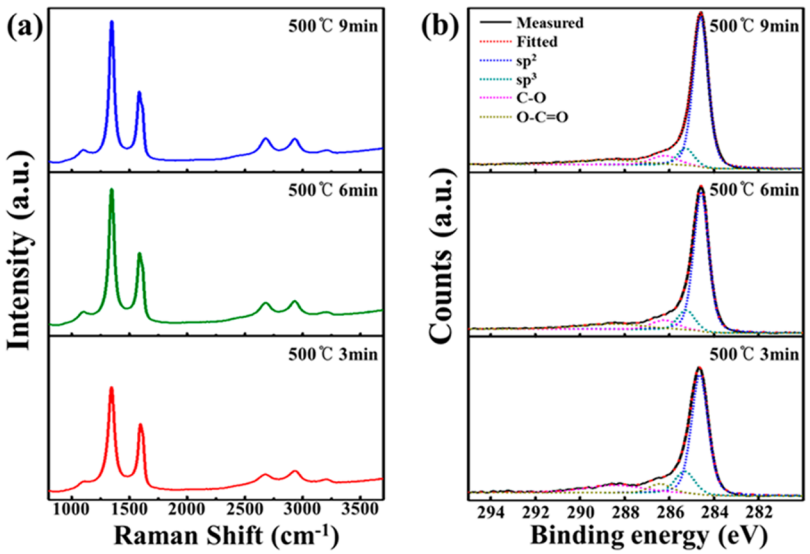

Figure 3. (a) Raman spectra of CuNW-G core−shell nanostructures that were treated at 500 °C and different LT-PECVD processing times (excitation wavelength: 532 nm). (b) High-resolution C 1s spectra of CuNW-G core−shell nanostructures prepared by LT-PECVD at 500 °C and different processing times.

of the graphene.[26,27] To obtain an atomically resolved lattice image of graphene, an inverse fast Fourier transform (FFT) was also performed on the selected area (Figure 2b). A hexagonal arrangement of carbon rings is clearly observed in the inverse FFT image. The distance between two carbon atoms is estimated to be 0.143 nm, demonstrating the growth of the nanocrystalline graphene. These TEM results clearly confirm that the CuNW-G core−shell nanostructure can be successfully synthesized at process temperatures as low as 400 °C by the LT-PECVD process. This is noteworthy because it is the first synthesis of the CuNW-G core−shell nanostructure by the LT-PECVD process.

The presence of graphene and the degree of the defect level in the CuNW-G core−shell nanostructure were investigated by Raman spectroscopy. Figure 3a displays the Raman spectra of the CuNW-G core−shell nanostructure measured at an excitation wavelength of 532 nm. They show typical G and 2D bands of graphene around ∼1580 and ∼2680 cm^{-1}, respectively. The 2D band represents the double-resonant Raman scattering, while the G band is generated by the E_{2g} phonon at the center of the Brillouin zone. The appearance of both G and 2D bands signifies that the graphene shell is successfully grown on the CuNW by the LT-PECVD process. It is also observed that the G band is much stronger than the 2D band, indicating that the synthesized graphene shell is grown as multilayered. However, a strong D band originating from structural disorder and defects is also observed around 1340 cm^{-1}. The intensity of the D band is relatively strong (I_D/I_G = 1.874), while the 2D band appears weak (I_G/I_{2D} = 0.425). Moreover, the G band tends to be shifted down as LT-PECVD processing time increases, as shown in Table S1. It has been reported that the shifted G band indicates random formation of nanocrystalline graphene islands, representing the increase of graphene domains.[24] These results clearly verify that nanocrystalline graphene domains in the CuNW-G core−shell nanostructure have a large number of edge states relative to the bulk graphene structure, leading to the strong intensity in the D band.[28]

The presence of carbon atoms and quantification of sp^2/sp^3 hybridization ratio in the CuNW-G core−shell nanostructure were also confirmed by X-ray photoelectron spectroscopy (XPS). Figure 3b displays the high-resolution C 1s spectra of the CuNW-G core−shell nanostructure prepared by the LT-PECVD process at 500 °C and different processing times. The C 1s scan spectrum of the CuNW-G core−shell nanostructure shows a pronounced C sp^2 peak centered at 284.58 eV, indicating that most of carbon atoms in the graphene shell are arranged in a two-dimensional graphite-like honeycomb lattice.[29] The relatively small C sp^3 peak is located at 285.24 eV, which is attributed to either intrinsic sp^3 defects or the edge of an individual graphene shell. The very small peaks at 286.23 and 288.51 eV could be attributed to oxygenated carbon structures such as C−O and O−C═O, respectively, indicating that the edges and defects of the graphene lattice have chemical bonds with oxygen.[30] Furthermore, it is observed that the ratio of the sp^2 peak in C 1s spectra increases from 63.4 to 72.7% as LT-PECVD processing temperature and time increases, suggesting that the nanocrystalline graphene structure in the CuNW-G core−shell nanostructure could be enhanced by controlling LT-PECVD process conditions, as shown in Table S2.[31]

To evaluate the CuNW-G core−shell nanostructure as a material for TCE, CuNW- and CuNW-G-based TCEs were fabricated. For the CuNW TCE, a CuNW ink was first prepared by dispersion of the CuNW in a mixture of organic solvents. Then, a CuNW TCE was prepared by

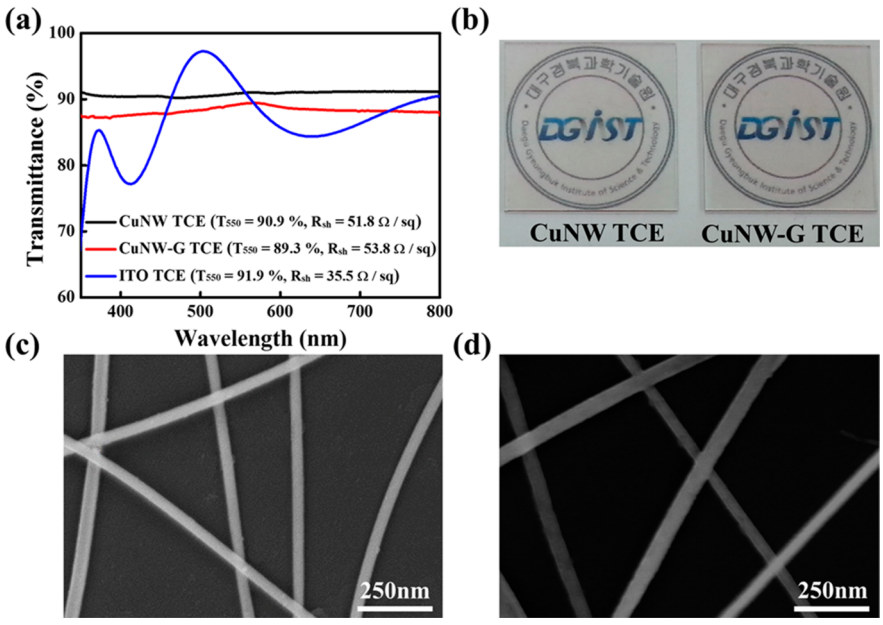

Figure 4. (a) UV/vis spectra of CuNW, CuNW-G, and ITO TCEs. (b) Photographs of CuNW (left) and CuNW-G (right) TCEs. SEM images of (c) CuNW and (d) CuNW-G TCEs.

spray-coating the CuNW ink on a glass substrate. For the CuNW-G TCE, it was treated with a mixed gas of CH_4 and H_2 using the LT-PECVD process with RF power of 50 W at 500 °C for 6 min. We measured the optical transmittance and sheet resistance of the CuNW and CuNW-G TCEs using UV/vis spectroscopy and a noncontact sheet measurement system. Generally, a conventional four-point probe method cannot measure the sheet resistance of the metal-nanowire-based TCE correctly when the sharp tip of the probe touches open spaces of the percolation network in the metal-nanowire-based TCE. Thus, we utilized a noncontact sheet resistance measurement method to precisely obtain the sheet resistance of both TCEs. As shown in Figure 4a, the optical transmittance and sheet resistance of the CuNW TCE are 90.9% at 550 nm and 51.8 Ω/sq, while those of the CuNW-G TCE are 89.3% at 550 nm and 53.8 Ω/sq. It is also found that both films possess relatively high optical transmittance in the visible wavelength region compared to ITO film. In addition, the optical transmittance of both films is almost constant in the near-infrared regions, indicating that high transmittance in a broad range of wavelengths allows the CuNW TCE to be used for a variety of optoelectronic devices. Compared to the CuNW TCE, slightly increased sheet resistance and reduced optical transmittance of the CuNW-G TCE could be attributed to additional light absorption of the graphene shell. However, the optical transmittance and sheet resistance of the CuNW-G TCE are still comparable to those of a conventional ITO TCE.

To evaluate the gas-barrier effect of the graphene shell on the thermal oxidation stability of the CuNW-G TCE, the CuNW and CuNW-G TCEs were placed in ambient conditions for 30 days. The sheet resistance

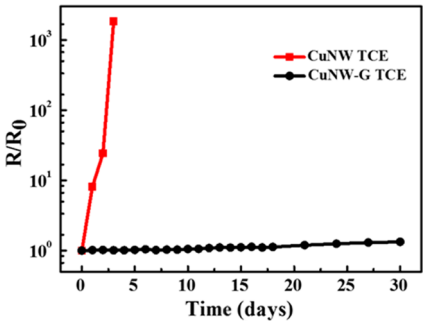

Figure 5. Sheet resistance changes of CuNW and CuNW-G TCEs during a stability test in air at room temperature for 30 days.

of both samples was monitored every day. Figure 5 presents the changes in sheet resistance of both samples during the thermal oxidation stability test. The sheet resistance of the CuNW TCE drastically increases over 1800 times within 2 days. However, the sheet resistance of the CuNW-G TCE increases slightly less than 9% even after 30 days. Furthermore, when they were exposed to the conditions of higher temperature and humidity (70 °C/70% RH), the sheet resistance of the CuNW TCEs increased over 76 times in 30 min. However, the sheet resistance of the CuNW-G TCEs showed a slight increase of less than 27% even after 120 h (Figure S10). It is noteworthy that this is the best thermal oxidation stability ever achieved in CuNW-based TCEs. The extremely enhanced thermal oxidation stability of the CuNW-G TCE clearly verifies that the graphene shell ensures long-term stability for the CuNW core for practical applications.

To investigate the reason for the remarkably enhanced thermal oxidation stability of the CuNW-G TCE, the surfaces of both films were investigated with SEM, X-ray diffraction (XRD), and XPS measurements.

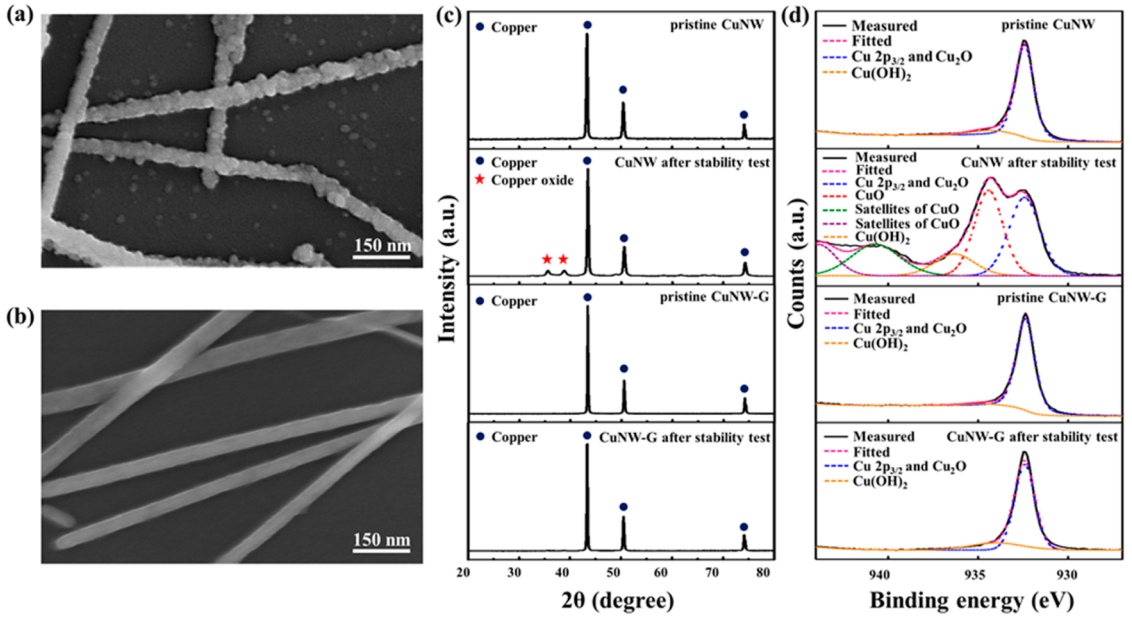

Figure 6. SEM images of (a) CuNW and (b) CuNW-G TCEs after the stability test. (c) XRD and (d) XPS spectra of CuNW and CuNW-G TCEs before and after the stability test.

As shown in Figure 6a, for the CuNW TCE, the formation of copper oxides on the surface of the CuNW is clearly observed. When the CuNW is oxidized, the electrical resistivity and junction resistance of the CuNW tend to increase, leading to the highly increased sheet resistance. On the contrary, for the CuNW-G TCE, there is no significant change on the morphology, indicating the successful protection of the CuNW by a graphene shell (Figure 6b). This is attributed to remarkable gas and moisture barrier properties of the graphene shell. XRD and XPS spectra were investigated to characterize the compositional changes of both samples during the thermal oxidation stability test. For the CuNW TCE, pronounced XRD peaks were observed at 35.7 and 39.0°, which are indicative of CuO and Cu_2O. In contrast, for the CuNW-G TCE, XRD peak intensities of CuO and Cu_2O are almost negligible. XPS results of both samples are consistent with XRD measurements. For the CuNW TCE, a pronounced XRD peak corresponding to CuO was observed at 934.4 eV. In addition, shakeup satellites of CuO were observed at 940.7 and 943.9 eV. On the other hand, the CuNW-G TCE did not show any strong XPS peaks from CuO and Cu_2O, revealing that moisture and oxygen could not permeate the graphene shell. As a result, the CuNW-G TCE barely shows any change of sheet resistance compared to the CuNW TCE, demonstrating that the graphene shell can encapsulate the CuNW core completely and protect the CuNW core from oxidation, resulting in a greatly improved long-term stability of the CuNW-G TCE.

Furthermore, the enhanced oxidation stability of CuNW-G nanostructure was also proven at the harsh conditions such as dispersion in deionized (DI) water. The CuNW and CuNW-G samples were dipped into DI water for 1 day. The color change of both samples was observed. The color of the CuNW-G solution has no significant change, suggesting that the graphene shell successfully protects the CuNW core from oxidation (Figure S11). In contrast, the color of CuNW changes from red to black due to the formation of copper oxides. We also prepared a CuNW TCE using a DI-water-treated CuNW sample and compared its sheet resistance with that of a CuNW TCE without DI water treatment. The sheet resistance of the CuNW TCE with DI water treatment was 125 times higher than that of the CuNW without DI water treatment. On the other hand, the sheet resistance of the CuNW-G TCE was almost the same regardless of DI water treatment. These results clearly indicate that the CuNW-G core–shell nanostructure possesses superior oxidation stability even in DI water because of the excellent gas and moisture barrier property of the graphene.

The potential suitability of the CuNW-G TCE was demonstrated by fabricating polymer solar cells. CuNW and CuNW-G TCEs were used as anode layers in bulk heterojunction (BHJ) PSCs. The optical transmittance and sheet resistance of the CuNW TCE are 79.8% at 550 nm and 32 Ω/sq, while those of the CuNW-G TCE are 79.0% at 550 nm and 36 Ω/sq. We examined the work function of CuNW and CuNW-G TCEs using ultraviolet photoelectron spectroscopy (UPS) (Figure S12). The work function values of the CuNW and CuNW-G TCEs are 4.33 and 4.50 eV, respectively. The BHJ PSCs were fabricated with a structure of CuNW or CuNW-G/PEDOT:PSS/PTB7:$PC_{71}BM$(1:1.5)/LiF/Al (Figure 7a). The active layers of polymer composites were spin-coated from polymer/$PC_{71}BM$ solutions prepared in chlorobenzene and 1,8-diiodooctane (3% v/v). The active

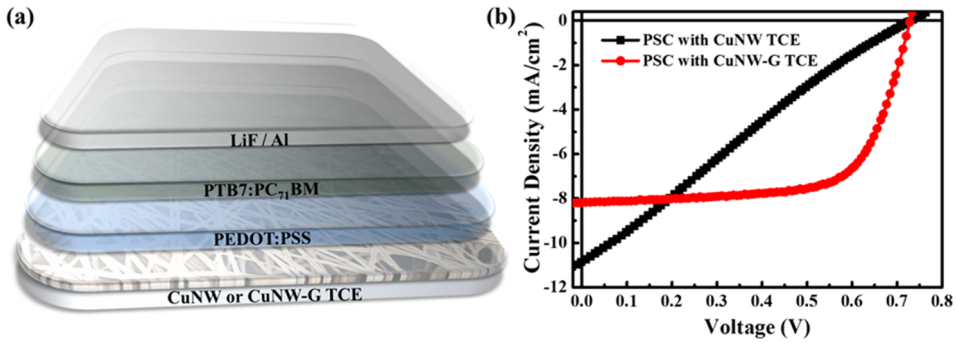

Figure 7. (a) Device architecture of the bulk heterojunction polymer solar cells based on the CuNW or CuNW-G TCE. (b) Current density−voltage (*J*−*V*) characteristics of bulk heterojunction polymer solar cells based on CuNW and CuNW-G TCEs.

layer thickness is about 80 nm. Figure 7b shows current density−voltage (*J*−*V*) characteristics of BHJ PSCs with CuNW and CuNW-G TCEs under AM 1.5 G illumination (100 mW cm^{-2}). The BHJ PSC with CuNW-G TCE exhibits a power conversion efficiency (PCE) of 4.04%, with an open-circuit voltage (V_{oc}) of 0.73 V, a short-circuit current density (J_{sc}) of 8.20 mA cm^{-2}, and a fill factor (FF) of 67.8%. On the other hand, the control device with CuNW TCE shows a PCE of 1.90% with an V_{oc} of 0.73 V, a J_{sc} of 10.84 $mAcm^{-2}$, and a FF of 24.1%. These results clearly indicate that PSC with CuNW-G TCE performs much better than that with CuNW TCE. Compared to the control device, the improvement in the photovoltaic performance of the devices with CuNW-G TCE mainly results from a highly enhanced FF value. Although PEDOT:PSS is a good material for planarization as well as hole extraction, its hygroscopic and acidic properties tend to make an unfavorable environment for CuNW TCEs. Consequently, some CuNWs are oxidized and etched out due to acidic PEDOT:PSS, resulting in severely reduced electrical properties. However, CuNW-G TCE shows excellent chemical resistance against acidic corrosion, confirming that the graphene shell provides chemical inertness against acidic conditions (Figure S13). Thus, the enhanced chemical stability of CuNW-G TCE is the most likely reason for enhancement of power conversion efficiency in PSCs.

CONCLUSION

In summary, we successfully synthesized a copper nanowire−graphene (CuNW-G) core−shell nanostructure by a LT-PECVD process at a temperature as low as 400 °C for the first time. The CuNW-G core−shell nanostructure was systematically characterized by SEM, TEM, XRD, Raman, and XPS measurements. A transparent conducting electrode based on the CuNW-G core−shell nanostructure exhibited excellent optical and electrical properties comparable to those of conventional ITO. In addition, it showed remarkable thermal oxidation and chemical stabilities because of the tight encapsulation of the CuNW with gas-impermeable graphene shells. The sheet resistance of the CuNW-G TCE increased slightly less than 9% even after 30 days in air, while that of the CuNW TCE increased over 1800 times within 2 days. The potential suitability of CuNW-G TCE was demonstrated by fabricating bulk heterojunction polymer solar cells. Polymer solar cells with CuNW-G TCE exhibited power conversion efficiency higher than those with CuNW TCE because of a significantly enhanced anticorrosion property. We anticipate that the CuNW-G core−shell nanostructure can be used as a potential alternative to conventional TCE materials for emerging optoelectronic devices such as flexible solar cells, displays, and touch panels.

METHODS

Synthesis of CuNW. $CuCl_2 \cdot 2H_2O$ (189 mg, 1.11 mmol), hexadecylamine (1296 mg, 5.37 mmol), and glucose (450 mg, 2.50 mmol) were dissolved in deionized water (30 mL). This mixture was stirred at room temperature overnight. Then, the reaction mixture was heated at 100 °C and stirred for 6 h. The color of the solution changed from blue to red brown. After the reaction, the suspension was washed with hot DI water (60 °C). To remove the excess HDA and glucose, the suspension was centrifuged for several cycles. Subsequently, the CuNW was rinsed in hexane and isopropyl alcohol (IPA) with a centrifuge. Then, the precipitates of the CuNW were dispersed in IPA. The dispersed CuNWs in IPA were filtered through a cellulose acetate membrane filter and dried in nitrogen gas. The dried CuNWs were stored in vacuum.

Fabrication of CuNW TCEs. CuNW ink was first prepared by dispersion of the CuNW in a mixture of organic solvents such as acetone (7.4 mL), ethanol (7.6 mL), ethyl acetate (3.5 mL), isopropyl alcohol (2.5 mL), and toluene (4 mL). To disperse the CuNWs in organic solvents, the CuNW ink was briefly ultrasonicated for 5 min. Then, a CuNW TCE was prepared by spray-coating the CuNW ink on a glass substrate with nitrogen gas at 60 °C. The CuNW TCE was pressed at 20 MPa and then annealed in a N_2-filled glovebox at 300 °C for 1 h.

Synthesis of CuNW-G Core−Shell Nanostructures and TCE Using LT-PECVD. A CuNW or CuNW TCE on a glass substrate was placed in a vacuum PECVD chamber (5.0×10^{-6} Torr) and heated to a process temperature ranging from 400 to 800 °C. We applied a hydrogen plasma with radio frequency power of 50 W for 3 min in order to remove an oxide layer and other contaminants on

the surface of the CuNW. Then, we introduced a reaction gas mixture composed of methane and hydrogen (CH_4/H_2 = 40:1, 120 sccm) into the chamber. We then performed PECVD at 1.0×10^{-3} Torr with RF power of 50 W for various process time ranging from 3 to 9 min and cooled to room temperature.

Fabrication of Bulk Heterojunction Polymer Solar Cells Based on CuNW and CuNW-G TCEs. Bulk heterojunction polymer solar cells are prepared as follows. An ITO-coated glass was cleaned by ultrasonic treatment in acetone, DI water, and isopropyl alcohol and dried by using nitrogen gas. The cleaned ITO-coated glass was treated in a UV-ozone chamber for 20 min. Then, poly(3,4-ethylenedioxythiophene):poly(styrenesulfonate) (PEDOT:PSS, CLEVIOS, AI4083) with 0.1% v/v Zonyl (Aldrich, FSO-100) was spin-coated onto CuNW or CuNW-G TCE in a N_2-purged glovebox. The PEDOT:PSS-coated CuNW or CuNW-G TCE was annealed on a hot plate at 120 °C for 10 min to remove the solvent. The thickness of the PEDOT:PSS layer was approximately 50 nm. PTB7 and [6,6]-phenyl-C_{71}-butyric acid methyl ester ($PC_{71}BM$) (1:1.5) were dissolved in chlorobenzene with 1,8-diiodooctane (3% v/v). Then, PTB7:$PC_{71}BM$ solution was spin-coated on top of the PEDOT:PSS layer and dried 20 min at room temperature in the glovebox. Finally, a cathode layer composed of LiF (1 nm) and Al (120 nm) was deposited by thermal evaporation ($<10^{-6}$ Torr). Therefore, we fabricated the polymer solar cells with different transparent electrode (CuNW or CuNW-G TCE)/PEDOT:PSS(50 nm)/PTB7:$PC_{71}BM$(80 nm)/LiF(1 nm)/Al(120 nm) configuration.

Characterization. HITACH S-4800 SEM was used to investigate the morphology of CuNWs and CuNW-G nanostructures. To coat the CuNW on a glass substrate, an ANEST IWATA HP-CP spray gun was used with N_2 gas. The CuNW and CuNW-G were observed with a field emission transmission electron microscope (HITACH HF-3300). The sheet resistances were measured by a NAPSON Corp. EC-80 noncontact measurement instrument. The optical transmittance of CuNW and CuNW-G TCEs was taken with a UV/vis spectrophotometer (Agilent Cary 100). XRD spectra of CuNW and CuNW-G were measured using Panalytical Empyrean. Raman spectra were obtained using a Raman spectrometer (Almega XR, Thermo Scientific) at an excitation wavelength of 532 nm. XPS spectra were acquired in an XPS microprobe (ESCALAB 250Xi, Thermo Scientific). The UPS measurements of CuNW and CuNW-G TCEs were carried out in an ultraspectrometer (ESCALAB 250Xi, Thermo Scientific) using a He I (21.2 eV) discharge lamp. The current−voltage ($J-V$) characteristics were measured using a solar simulator (K-3300, McScience) in the air without a device encapsulation. One sun light intensity (100 mW cm^{-2}) was calibrated using a c-Si photodiode (K801S-K13, McScience) as a standard.

Conflict of Interest: The authors declare no competing financial interest.

Acknowledgment. This research was supported by Basic Science Research Program through the National Research Foundation of Korea (NRF) funded by the Ministry of Education, Science, and Technology (2012R1A1A1040811). This work was also supported by the DGIST MIREBraiN Program and DGIST R&D Program of Ministry of Science, ICT and Future Planning of Korea (15-BD-0404, 14-HRSS-01).

Supporting Information Available: Synthesis and characterization of CuNWs and CuNW-G core−shell nanostructures; additional information on Raman spectra and XPS data; and stability tests of CuNWs and CuNW-G core−shell nanostructures. This material is available free of charge *via* the Internet at http://pubs.acs.org.

REFERENCES AND NOTES

1. Wu, H.; Kong, D.; Ruan, Z.; Hsu, P.-C.; Wang, S.; Yu, Z.; Carney, T. J.; Hu, L.; Fan, S.; Cui, Y. A Transparent Electrode Based on a Metal Nanotrough Network. *Nat. Nanotechnol.* **2013**, *8*, 421–425.
2. Lee, H.; Lee, D.; Ahn, Y.; Lee, E.-W.; Park, L. S.; Lee, Y. Highly Efficient and Low Voltage Silver Nanowire-Based OLEDs Employing a n-Type Hole Injection Layer. *Nanoscale* **2014**, *6*, 8565–8570.
3. Salvatierra, R. V.; Cava, C. E.; Roman, L. S.; Zarbin, A. J. G. ITO-Free and Flexible Organic Photovoltaic Device Based on High Transparent and Conductive Polyaniline/Carbon Nanotube Thin Films. *Adv. Funct. Mater.* **2013**, *23*, 1490–1499.
4. Zhu, R.; Chung, C.-H.; Cha, K. C.; Yang, W.; Zheng, Y. B.; Zhou, H.; Song, T.-B.; Chen, C.-C.; Weiss, P. S.; Li, G.; et al. Fused Silver Nanowires with Metal Oxide Nanoparticles and Organic Polymers for Highly Transparent Conductors. *ACS Nano* **2011**, *5*, 9877–9882.
5. van de Groep, J.; Spinelli, P.; Polman, A. Transparent Conducting Silver Nanowire Networks. *Nano Lett.* **2012**, *12*, 3138–3144.
6. Hecht, D. S.; Hu, L.; Irvin, G. Emerging Transparent Electrodes Based on Thin Films of Carbon Nanotubes, Graphene, and Metallic Nanostructures. *Adv. Mater.* **2011**, *23*, 1482–1513.
7. Kim, Y. H.; Sachse, C.; Machala, M. L.; May, C.; Müller-Meskamp, L.; Leo, K. Highly Conductive PEDOT:PSS Electrode with Optimized Solvent and Thermal Post-treatment for ITO-Free Organic Solar Cells. *Adv. Funct. Mater.* **2011**, *21*, 1076–1081.
8. Leem, D. S.; Edwards, A.; Faist, M.; Nelson, J.; Bradley, D. D. C; de Mello, J. C. Efficient Organic Solar Cells with Solution-Processed Silver Nanowire Electrodes. *Adv. Mater.* **2011**, *23*, 4371–4375.
9. Lee, D.; Lee, H.; Ahn, Y.; Lee, Y. High-Performance Flexible Transparent Conductive Film Based on Graphene/AgNW/Graphene Sandwich Structure. *Carbon* **2015**, *81*, 439–446.
10. Xu, F.; Zhu, Y. Highly Conductive and Stretchable Silver Nanowire Conductors. *Adv. Mater.* **2012**, *24*, 5117–5122.
11. Ahn, Y.; Jeong, Y.; Lee, Y. Improved Thermal Oxidation Stability of Solution-Processable Silver Nanowire Transparent Electrode by Reduced Graphene Oxide. *ACS Appl. Mater. Interfaces* **2012**, *4*, 6410–6414.
12. Ahn, Y.; Lee, H.; Lee, D.; Lee, Y. Highly Conductive and Flexible Silver Nanowires-Based Microelectrodes on Biocompatible Hydrogel. *ACS Appl. Mater. Interfaces* **2014**, *6*, 18401–18407.
13. Rathmell, A. R.; Wiley, B. J. The Synthesis and Coating of Long, Thin Copper Nanowires To Make Flexible, Transparent Conducting Films on Plastic Substrates. *Adv. Mater.* **2011**, *23*, 4798–4803.
14. Sachse, C.; Weiß, N.; Gaponik, N.; Müller-Meskamp, L.; Eychmüller, A.; Leo, K. ITO-Free, Small-Molecule Organic Solar Cells on Spray-Coated Copper-Nanowire-Based Transparent Electrodes. *Adv. Energy Mater.* **2014**, *4*, 1300737.
15. Ye, S.; Rathmell, A. R.; Stewart, I. E.; Ha, Y.-C.; Wilson, A. R.; Chen, Z.; Wiley, B. J. A Rapid Synthesis of High Aspect Ratio Copper Nanowires for High-Performance Transparent Conducting Films. *Chem. Commun.* **2014**, *50*, 2562–2564.
16. Zhang, D.; Wang, R.; Wen, M.; Weng, D.; Cui, X.; Sun, J.; Li, H.; Lu, Y. Synthesis of Ultralong Copper Nanowires for High-Performance Transparent Electrodes. *J. Am. Chem. Soc.* **2012**, *134*, 14283–14286.
17. Stewart, I. E.; Rathmell, A. R.; Yan, L.; Ye, S.; Flowers, P. F.; You, W.; Wiley, B. J. Solution-Processed Copper−Nickel Nanowire Anodes for Organic Solar Cells. *Nanoscale* **2014**, *6*, 5980–5988.
18. Hsu, P.-C.; Wu, H.; Carney, T. J.; McDowell, M. T.; Yang, Y.; Garnett, E. C.; Li, M.; Hu, L.; Cui, Y. Passivation Coating on Electrospun Copper Nanofibers for Stable Transparent Electrodes. *ACS Nano* **2012**, *6*, 5150–5156.
19. Chen, J.; Zhou, W.; Chen, J.; Fan, Y.; Zhang, Z.; Huang, Z.; Feng, X.; Mi, B.; Ma, Y.; Huang, W. Solution-Processed Copper Nanowire Flexible Transparent Electrodes with PEDOT:PSS as Binder, Protector and Oxide-Layer Scavenger for Polymer Solar Cells. *Nano Res.* **2014**, 1–9.
20. Lee, D.; Lee, H.; Ahn, Y.; Jeong, Y.; Lee, D.-Y.; Lee, Y. Highly Stable and Flexible Silver Nanowire−Graphene Hybrid Transparent Conducting Electrodes for Emerging Optoelectronic Devices. *Nanoscale* **2013**, *5*, 7750–7755.
21. Li, X.; Cai, W.; An, J.; Kim, S.; Nah, J.; Yang, D.; Piner, R.; Velamakanni, A.; Jung, I.; Tutuc, E.; et al. Large-Area Synthesis of High-Quality and Uniform Graphene Films on Copper Foils. *Science* **2009**, *324*, 1312–1314.

22. Kim, Y. S.; Lee, J. H.; Kim, Y. D.; Jerng, S.-K.; Joo, K.; Kim, E.; Jung, J.; Yoon, E.; Park, Y. D.; Seo, S.; et al. Methane as an Effective Hydrogen Source for Single-Layer Graphene Synthesis on Cu Foil by Plasma Enhanced Chemical Vapor Deposition. *Nanoscale* **2013**, *5*, 1221–1226.
23. Battaglia, C.; Escarré, J.; Söderström, K.; Charrière, M.; Despeisse, M.; Haug, F.-J.; Ballif, C. Nanomoulding of Transparent Zinc Oxide Electrodes for Efficient Light Trapping in Solar Cells. *Nat. Photonics* **2011**, *5*, 535–538.
24. Yang, C.; Bi, H.; Wan, D.; Huang, F.; Xie, X.; Jiang, M. Direct PECVD Growth of Vertically Erected Graphene Walls on Dielectric Substrates as Excellent Multifunctional Electrodes. *J. Mater. Chem. A* **2013**, *1*, 770–775.
25. Lee, C. S.; Cojocaru, C. S.; Moujahid, W.; Lebental, B.; Chaigneau, M.; Châtelet, M.; Le Normand, F.; Maurice, J.-L. Synthesis of Conducting Transparent Few-Layer Graphene Directly on Glass at 450°C. *Nanotechnology* **2012**, *23*, 265603.
26. Gu, W.; Zhang, W.; Li, X.; Zhu, H.; Wei, J.; Li, Z.; Shu, Q.; Wang, C.; Wang, K.; Shen, W.; et al. Graphene Sheets from Worm-like Exfoliated Graphite. *J. Mater. Chem.* **2009**, *19*, 3367–3369.
27. Cong, C.; Li, K.; Zhang, X. X.; Yu, T. Visualization of Arrangements of Carbon Atoms in Graphene Layers by Raman Mapping and Atomic-Resolution TEM. *Sci. Rep.* **2013**, *3*, 1195.
28. Rummeli, M. H.; Bachmatiuk, A.; Scott, A.; Borrnert, F.; Warner, J. H.; Hoffman, V.; Lin, J.-H.; Cuniberti, G.; Buchner, B. Direct Low-Temperature Nanographene CVD Synthesis over a Dielectric Insulator. *ACS Nano* **2010**, *4*, 4206–4210.
29. Allen, M. J.; Tung, V. C.; Kaner, R. B. Honeycomb Carbon: A Review of Graphene. *Chem. Rev.* **2010**, *110*, 132–145.
30. Hawaldar, R.; Merino, P.; Correia, M. R.; Bdikin, I.; Grácio, J.; Méndez, J.; Martín-Gago, J. A.; Singh, M. K. Large-Area High-Throughput Synthesis of Monolayer Graphene Sheet by Hot Filament Thermal Chemical Vapor Deposition. *Sci. Rep.* **2012**, *2*, 682.
31. Ermolieff, A.; Chabli, A.; Pierre, F.; Rolland, G.; Rouchon, D.; Vannuffel, C.; Vergnaud, C.; Baylet, J.; Semeria, M. N. XPS, Raman Spectroscopy, X-ray Diffraction, Specular X-ray Reflectivity, Transmission Electron Microscopy and Elastic Recoil Detection Analysis of Emissive Carbon Film Characterization. *Surf. Interface Anal.* **2001**, *31*, 185–190.